Study of muons from ultrahigh energy cosmic ray air showers measured with the Telescope Array experiment

R. U. Abbasi,[1] M. Abe,[2] T. Abu-Zayyad,[1] M. Allen,[1] R. Azuma,[3] E. Barcikowski,[1] J. W. Belz,[1] D. R. Bergman,[1]
S. A. Blake,[1] R. Cady,[1] B. G. Cheon,[4] J. Chiba,[5] M. Chikawa,[6] A. Di Matteo,[7] T. Fujii,[8] K. Fujita,[9] M. Fukushima,[8,10]
G. Furlich,[1] T. Goto,[9] W. Hanlon,[1] M. Hayashi,[11] Y. Hayashi,[9] N. Hayashida,[12] K. Hibino,[12] K. Honda,[13] D. Ikeda,[8]
N. Inoue,[2] T. Ishii,[13] R. Ishimori,[3] H. Ito,[14] D. Ivanov,[1] H. M. Jeong,[15] S. Jeong,[15] C. C. H. Jui,[1] K. Kadota,[16] F. Kakimoto,[3]
O. Kalashev,[17] K. Kasahara,[18] H. Kawai,[19] S. Kawakami,[9] S. Kawana,[2] K. Kawata,[8] E. Kido,[8] H. B. Kim,[4] J. H. Kim,[1]
J. H. Kim,[20] S. Kishigami,[9] S. Kitamura,[3] Y. Kitamura,[3] V. Kuzmin,[17,*] M. Kuznetsov,[17] Y. J. Kwon,[21] K. H. Lee,[15]
B. Lubsandorzhiev,[17] J. P. Lundquist,[1] K. Machida,[13] K. Martens,[10] T. Matsuyama,[9] J. N. Matthews,[1] R. Mayta,[9]
M. Minamino,[9] K. Mukai,[13] I. Myers,[1] K. Nagasawa,[2] S. Nagataki,[14] R. Nakamura,[22] T. Nakamura,[23] T. Nonaka,[8] H. Oda,[9]
S. Ogio,[9] J. Ogura,[3] M. Ohnishi,[8] H. Ohoka,[8] T. Okuda,[24] Y. Omura,[9] M. Ono,[14] R. Onogi,[9] A. Oshima,[9] S. Ozawa,[18]
I. H. Park,[15] M. S. Pshirkov,[17,25] J. Remington,[1] D. C. Rodriguez,[1] G. Rubtsov,[17] D. Ryu,[20] H. Sagawa,[8] R. Sahara,[9]
K. Saito,[8] Y. Saito,[22] N. Sakaki,[8] N. Sakurai,[9] L. M. Scott,[26] T. Seki,[22] K. Sekino,[8] P. D. Shah,[1] F. Shibata,[13] T. Shibata,[8]
H. Shimodaira,[8] B. K. Shin,[9] H. S. Shin,[8] J. D. Smith,[1] P. Sokolsky,[1] B. T. Stokes,[1] S. R. Stratton,[1,26] T. A. Stroman,[1]
T. Suzawa,[2] Y. Takagi,[9] Y. Takahashi,[9] M. Takamura,[5] M. Takeda,[8] R. Takeishi,[15,†] A. Taketa,[27] M. Takita,[8] Y. Tameda,[28]
H. Tanaka,[9] K. Tanaka,[29] M. Tanaka,[30] S. B. Thomas,[1] G. B. Thomson,[1] P. Tinyakov,[7,17] I. Tkachev,[17] H. Tokuno,[3]
T. Tomida,[22] S. Troitsky,[17] Y. Tsunesada,[9] K. Tsutsumi,[3] Y. Uchihori,[31] S. Udo,[12] F. Urban,[32] T. Wong,[1]
M. Yamamoto,[22] R. Yamane,[9] H. Yamaoka,[30] K. Yamazaki,[12] J. Yang,[33] K. Yashiro,[5] Y. Yoneda,[9]
S. Yoshida,[19] H. Yoshii,[34] Y. Zhezher,[17] and Z. Zundel[1]

(Telescope Array Collaboration)

[1]*High Energy Astrophysics Institute and Department of Physics and Astronomy, University of Utah,*
Salt Lake City, Utah, USA
[2]*The Graduate School of Science and Engineering, Saitama University, Saitama, Saitama, Japan*
[3]*Graduate School of Science and Engineering, Tokyo Institute of Technology, Meguro, Tokyo, Japan*
[4]*Department of Physics and The Research Institute of Natural Science, Hanyang University,*
Seongdong-gu, Seoul, Korea
[5]*Department of Physics, Tokyo University of Science, Noda, Chiba, Japan*
[6]*Department of Physics, Kindai University, Higashi Osaka, Osaka, Japan*
[7]*Service de Physique Théorique, Université Libre de Bruxelles, Brussels, Belgium*
[8]*Institute for Cosmic Ray Research, University of Tokyo, Kashiwa, Chiba, Japan*
[9]*Graduate School of Science, Osaka City University, Osaka, Osaka, Japan*
[10]*Kavli Institute for the Physics and Mathematics of the Universe (WPI), Todai Institutes for Advanced Study,*
the University of Tokyo, Kashiwa, Chiba, Japan
[11]*Information Engineering Graduate School of Science and Technology, Shinshu University,*
Nagano, Nagano, Japan
[12]*Faculty of Engineering, Kanagawa University, Yokohama, Kanagawa, Japan*
[13]*Interdisciplinary Graduate School of Medicine and Engineering, University of Yamanashi,*
Kofu, Yamanashi, Japan
[14]*Astrophysical Big Bang Laboratory, RIKEN, Wako, Saitama, Japan*
[15]*Department of Physics, Sungkyunkwan University, Jang-an-gu, Suwon, Korea*
[16]*Department of Physics, Tokyo City University, Setagaya-ku, Tokyo, Japan*
[17]*Institute for Nuclear Research of the Russian Academy of Sciences, Moscow, Russia*
[18]*Advanced Research Institute for Science and Engineering, Waseda University,*
Shinjuku-ku, Tokyo, Japan
[19]*Department of Physics, Chiba University, Chiba, Chiba, Japan*
[20]*Department of Physics, School of Natural Sciences, Ulsan National Institute of Science and Technology,*
UNIST-gil, Ulsan, Korea
[21]*Department of Physics, Yonsei University, Seodaemun-gu, Seoul, Korea*
[22]*Academic Assembly School of Science and Technology Institute of Engineering, Shinshu University,*
Nagano, Nagano, Japan
[23]*Faculty of Science, Kochi University, Kochi, Kochi, Japan*
[24]*Department of Physical Sciences, Ritsumeikan University, Kusatsu, Shiga, Japan*
[25]*Sternberg Astronomical Institute, Moscow M.V. Lomonosov State University, Moscow, Russia*

[26]*Department of Physics and Astronomy, Rutgers University—The State University of New Jersey,*
Piscataway, New Jersey, USA
[27]*Earthquake Research Institute, University of Tokyo, Bunkyo-ku, Tokyo, Japan*
[28]*Department of Engineering Science, Faculty of Engineering, Osaka Electro-Communication University,*
Neyagawa-shi, Osaka, Japan
[29]*Graduate School of Information Sciences, Hiroshima City University, Hiroshima, Hiroshima, Japan*
[30]*Institute of Particle and Nuclear Studies, KEK, Tsukuba, Ibaraki, Japan*
[31]*National Institute of Radiological Science, Chiba, Chiba, Japan*
[32]*CEICO, Institute of Physics, Czech Academy of Sciences Prague, Czech Republic*
[33]*Department of Physics and Institute for the Early Universe, Ewha Womans University,*
Seodaaemun-gu, Seoul, Korea
[34]*Department of Physics, Ehime University, Matsuyama, Ehime, Japan*

One of the uncertainties in the interpretation of ultrahigh energy cosmic ray data comes from the hadronic interaction models used for air shower Monte Carlo (MC) simulations. The number of muons observed at the ground from ultrahigh energy cosmic ray–induced air showers is expected to depend upon the hadronic interaction model. One may therefore test the hadronic interaction models by comparing the measured number of muons with the MC prediction. In this paper, we present the results of studies of muon densities in ultrahigh energy extensive air showers obtained by analyzing the signal of surface detector stations which should have high *muon purity*. The muon purity of a station will depend on both the inclination of the shower and the relative position of the station. In seven years' data from the Telescope Array experiment, we find that the number of particles observed for signals with an expected muon purity of $\sim 65\%$ at a lateral distance of 2000 m from the shower core is $1.72 \pm 0.10 (\text{stat}) \pm 0.37 (\text{syst})$ times larger than the MC prediction value using the QGSJET II-03 model for proton-induced showers. A similar effect is also seen in comparisons with other hadronic models such as QGSJET II-04, which shows a $1.67 \pm 0.10 \pm 0.36$ excess. We also studied the dependence of these excesses on lateral distances and found a slower decrease of the lateral distribution of muons in the data as compared to the MC, causing larger discrepancy at larger lateral distances.

I. INTRODUCTION

The origin of ultrahigh energy cosmic rays (UHECRs) has been a long-standing mystery of astrophysics. The Telescope Array (TA) experiment [1] in Utah, USA, is the largest experiment in the northern hemisphere observing UHECRs. It aims to reveal the origin of UHECRs by studying the energy spectrum, mass composition and anisotropy of cosmic rays. When a UHECR enters the atmosphere, it interacts with atmospheric nuclei and generates the particle cascade, which is called an air shower. The information of primary cosmic rays is estimated from observed signals of air shower particles and the air shower Monte Carlo (MC) simulation.

UHECR air showers are not fully understood. At present, the maximum energy of hadronic interactions in the target rest frame accessible at accelerators is 10^{17} eV at the CERN LHC. The MC for cosmic rays in the energies above 10^{18} eV uses the extrapolated values of the parameters

of hadronic interactions, such as the cross section and multiplicity. The values of these parameters differ between hadronic interaction models, due to the uncertainty of modeling pion or kaon generation at the early age of the air shower development. Thus, inferences of UHECR composition from air shower measurements are model dependent [2,3], which is important in understanding the origin of UHECRs because cosmic rays are deflected in the Galactic and extragalactic magnetic fields.

In addition to that, the HiRes/MIA experiment reported a deficit in the number of muons from MC air showers compared with experimental data for $E \gtrsim 10^{17}$ eV [4]. The Yakutsk experiment also indicated lower simulated muon densities than those observed for $E \gtrsim 10^{19}$ eV [5]. The Pierre Auger Observatory, which is located in Mendoza, Argentina, reported [6] a model-dependent deficit of muons in simulations of 30%–80% relative to the data, 10^{19} eV. The Pierre Auger Collaboration also reported that the observed hadronic signal in UHECR air showers is 1.61 ± 0.21 (1.33 ± 0.16) times larger than the post-LHC MC prediction values for QGSJET II-04 [7] (EPOS-LHC [8]), including statistical and systematic errors [9]. For $E \lesssim 10^{17}$ eV, The KASCADE-Grande experiment [10]

[*]Deceased.
[†]Corresponding author.
takeishi@skku.edu

and an atmospheric muon study [11] reported the discrepancy between experimental data and the air shower MC models, whereas the Icetop preliminary result [12] and the EAS-MSU array [13] showed no excess of muons in their data.

The analysis of air shower components provides the information to obtain a realistic air shower model. The number of muons from a UHECR on the ground depends on the mass composition of primary cosmic rays. The MC prediction depends also on hadronic interaction models since it has information about the shower development at an early stage. One may test the hadronic interaction models by comparing the measured number of muons with the MC prediction. Furthermore, the lateral distribution of muons—which was not analyzed in the previous studies [4–6,9]—contains information about the hadronic interaction. In this work, we study the difference between the number of muons in experimental data and the MC. We also study the difference as a function of lateral distance from the shower core. For that, an analysis for muons from UHECR air showers with the TA surface detectors (SDs) was developed.

II. TELESCOPE ARRAY EXPERIMENT

A. Detector and data taking

The TA experiment is designed to measure air shower particles on the ground with the SDs and fluorescence light induced by the air shower with the fluorescence detectors (FDs). The TA SD array consists of 507 scintillation counters, placed on a square grid with 1.2 km spacing, covering 700 km^2 [14]. Each TA SD is composed of two layers of plastic scintillator with two photomultiplier tubes (PMTs), one for each layer. It has an area of 3 m^2, and each layer has 1.2 cm thickness. The scintillators and PMTs are contained in a stainless steel box which is mounted under a 1.2 mm thick iron roof to protect the detector from large temperature variations. The SD station is solar powered, and data are collected by a wireless local-area network system. The station measures air shower particles by collecting photons generated in scintillators through wavelength shifting fibers and detecting them with PMTs. The signals from PMTs are digitized by a commercial 12-bit flash analog-digital converter (FADC) with a 50 MHz sampling rate on the CPU board. The SD array trigger is created when at least three adjacent counters detect energy deposits equivalent to or greater than the equivalent of three minimum ionizing particles (MIPs) within 8 μs. The readout system then records SD signals equivalent to $\gtrsim 0.3$ MIP detected within ± 32 μs of the trigger time. The trigger efficiency is greater than 97% for primary particles with energies above 10^{19} eV [14]. The calibration is performed every 10 min by monitoring histograms of signals from single atmospheric muons and comparing them with simulated distributions of energy

deposition [14], thus determining the correlation between the FADC values and the energy deposition.

The three TA FD stations are located around the SD array and view the sky above the array [15]. The stations consist of 38 telescopes with spherical mirrors. The fluorescence light from air showers is collected by the mirror and detected by PMTs through a UV bandpass filter. The signals from each PMT are digitized by a 12-bit FADC with a 40 MHz sampling rate. The trigger electronics select a track pattern of triggered PMTs in real time and record air shower tracks.

B. Event reconstruction

The TA SD event reconstruction consists of the following steps [16]. First, SD signals that are related to air shower events are selected by determining a cluster which is contiguous in space and time. Signals less than about 1.4 vertical equivalent muon (VEM) are excluded from the cluster. This process reduces background signals from the random atmospheric muons, which occur uniformly in space and time at a rate of 0.05 per station within one event time period (± 32 μs). Second, a time fit of shower arrivals at the SDs is performed to determine the geometry of cosmic ray air showers. Third, the lateral distribution of charged particle densities at the SDs is fit using a lateral distribution function of the AGASA experiment [17,18] to determine $S800$, the density of shower particles at a lateral distance of 800 m from the air shower axis. The energy of the cosmic ray is estimated by using a look-up table in $S800$ and the shower zenith angle. The table is obtained by a large statistics MC simulation using CORSIKA [19] and the QGSJET II-03 hadronic model. Finally, the reconstructed energy is scaled to the energy measured by the TA FD, which is determined using calorimetric detection of an air shower energy deposition in the atmosphere [15,20,21] with less hadronic interaction dependence than the SD. The energy and angular resolutions for a primary energy within 10$^{18.5}$ eV $< E <$ 10$^{19.0}$ eV are 29% and 2.1°, respectively [22]. Those for energies above 10^{19} eV are 19% and 1.4°, respectively. The resolution of the distance from a shower axis is about 70–80 m within 10$^{18.8}$ eV $< E <$ 10$^{19.2}$ eV, which is the energy range analyzed in this work.

III. MONTE CARLO SIMULATION

We use CORSIKA6.960 and QGSJET II-03 as a reference model for high energy hadronic interactions. The MCs for other models are also generated using the same MC procedure. We also use FLUKA2008.3C [23,24] to model low energy hadronic interactions and EGS4 [25] to model electromagnetic interactions. The thinning [26] and "de-thinning" [27] techniques are used to reduce the computation time. The detector simulation is performed by using GEANT4 [28] toolkit.

The simulated cosmic ray energies range from $10^{16.55}$ to $10^{20.55}$ eV. The simulated zenith angle is isotropically distributed from 0° to 60°. The azimuth angle and core position are randomly distributed within the SD array. The same reconstruction procedure as experimental data is applied for the MC data set. We sampled simulated events so that the energy distribution follows the spectrum measured by the HiRes experiment [29]. The distributions of the reconstructed shower parameters, such as energy and zenith angle distributions, are in good agreement between the experimental data and the MC [16].

IV. ANALYSIS PROCEDURE

A. Data set

We use the TA SD seven years' data set recorded from May 11, 2008, through May 11, 2015, and the events reconstructed by the same method as the TA spectrum analysis [30] with an energy range $10^{18.8}$ eV $< E < 10^{19.2}$ eV. In this energy range, the mass composition of the primary cosmic rays is consistent with a light component within statistical and systematic errors as determined by X_{max} measurement using the TA FD [2,3,20,31], where X_{max} is the depth in the atmosphere of air shower maximum; thus, we use the MC for proton primaries. We used the energy scale corrected by the FD (reconstructed energy scale) for the experimental data and the scale not corrected by the FD (thrown energy scale) for the MC. The correction factor is 27%, which corresponds to a difference of about 20%–30% in signal sizes of SDs at a lateral distance of 800 m. The experimental data are compared with the MC using the hadronic models QGSJET II-03, QGSJET II-04, EPOS1.99 [32] and SIBYLL2.1 [33].

B. Analysis framework

The TA SD, made of plastic scintillators [14], is sensitive to the electromagnetic (EM) component (electrons and gammas) that is the predominant part of secondary particles from the air showers. The conversion rate of gammas to electrons in the TA SD is ∼20% at 1 GeV. To increase the ratio of muons in SD signals, we used the following analysis approach. First, we define the condition of the high *muon purity* using the MC. Then, we compare the observed signal size from air shower particles with the MC prediction under the high muon purity condition.

The secondary particles generated in the atmosphere are attenuated by the interaction with atmospheric particles, and they decay before they reach the ground. The EM components experience greater attenuation than muons over the same path length, because the EM components largely lose their energy by the pair production and bremsstrahlung in the shower development but muons can penetrate the atmosphere down to the ground before their decay. Hence, the ratio of the energy deposit of air shower muons to that of all particles, which consist of air shower and background components, in SD signals
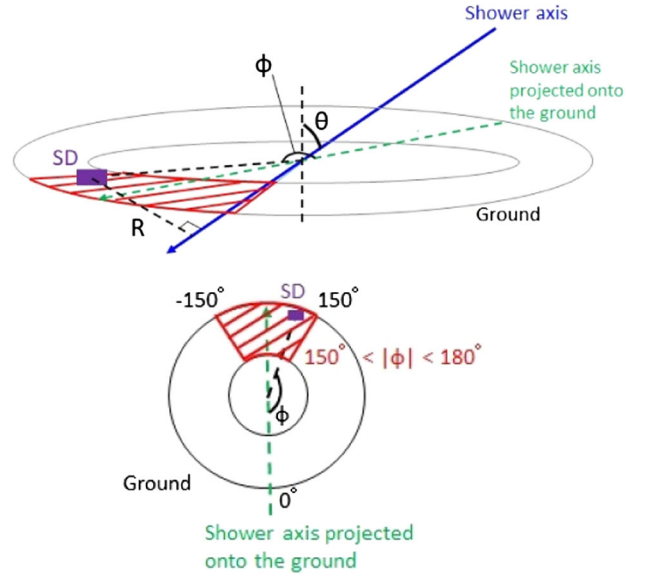

FIG. 1. (top) Geometry definition of the muon analysis. A SD location on the ground is selected by ϕ and R to reduce the EM background. The muon purity in the SD signal is calculated in each (ϕ, R) bin. There are six bins for ϕ and 18 bins for R from 500 to 4500 m. The red shaded region in the figure shows the bin for $150° < |\phi| < 180°$ where the distance from the particle generation points on the shower axis is relatively larger than other ϕ bins, which is expected to be the less EM background bin. (bottom) Top view for the ϕ definition.

(hereafter, this ratio is described as the muon purity) is expected to be larger for SDs more distant from secondary particle generation points on the shower axis. We classify the detector hits in the air shower events of the data set using θ (the zenith angle), ϕ (the azimuth angle relative to the shower arrival direction projected onto the ground) and R (the distance from a shower axis). The geometry definition is described in Fig. 1. When $\theta, |\phi|$ or R values become large, the path length of air shower particles increases, and then the muon purity in SD signals is expected to be high.

The integrated FADC is calculated for each SD participating in the event. The FADC count, converted to VEM units, is entered in the histogram of the corresponding (θ, ϕ, R) bin. Figures 2 and 3 show sample waveforms and histograms for each particle type. One detector signal corresponds to one entry in the histogram. An SD which has no signal is assigned to the 0 VEM bin of the histogram. Since the cut on hit signals less than about 1.4 VEM is applied to the total (black), there are remaining entries below the signal size for other components (other colors). Figure 4 shows the lateral distributions of SD signals and the muon purity. The muon purity is mainly 60%–70% on the high muon purity condition ($30° < \theta < 45°$, $150° < |\phi| < 180°$, 2000 m $< R < 4000$ m). We use these conditions to select high muon purity events for the comparison of the data with the MC.
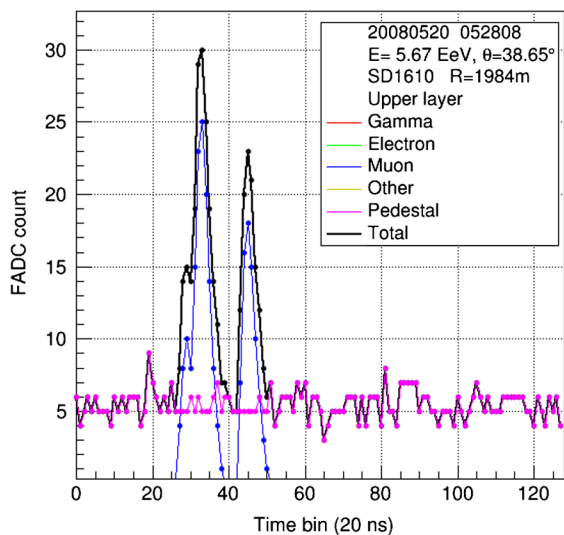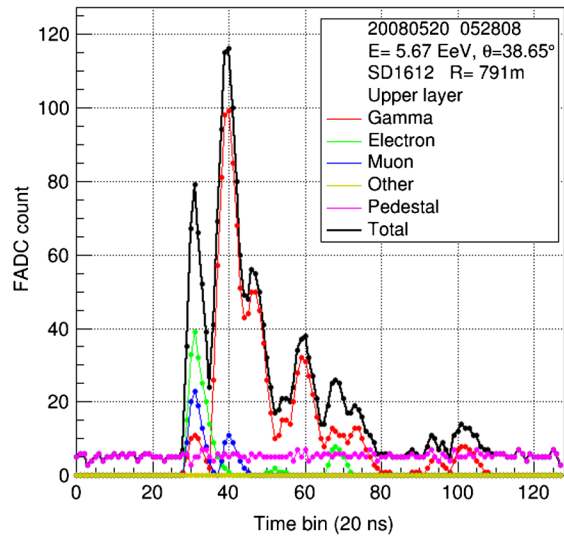
FIG. 2. (top) Sample event waveforms of different particle types in a SD (3 m² in area) at $R \simeq 800$ m made by the MC. The red, green, blue, yellow, magenta and black represent gamma, electron, muon, other shower components, atmospheric muon background and the total of them, respectively. (bottom) Same as top figure, but at $R \simeq 2000$ m. The components except muons and pedestals have 0 FADC values in this sample.

FIG. 3. (top) Histograms of the signal size (denoted as S in the figure) of different particle types in a SD made by the MC for $10^{18.8}$ eV $< E < 10^{19.2}$ eV, $0° < \theta < 30°$, $|\phi| < 30°$, 920 m $< R <$ 1040 m. The red, green, blue, yellow, magenta and black represent gamma, electron, muon, other shower components, atmospheric muon background and the total of them, respectively. (bottom) Same as the top figure, but for $30° < \theta < 45°$, $150° < |\phi| < 180°$, 1910 m $< R <$ 2160 m.

The statistical error of the average signal cannot be simply calculated for $R \gtrsim 1500$ m. It is because the average number of air shower particles is less than unity in the region, so the fraction of SDs with no hit signals is too large to determine lower and upper errors from the shape of the signal size distribution. Air shower particles reaching a SD are expected to be discrete and independent of each other, and hence we assume the Poisson distribution $f(x) = N^x e^{-N}/x!$; N is the average value of the distribution, and x is the variable for the signal size distribution. We calculated the average signal by the following equation: $n_0/n_{all} = f(0) = e^{-N}$. Here, n_0 and n_{all} are the entries of 0 VEM bin and the whole distribution, respectively. The

probability that zero values appear n_0 times in n_{all} samples follows the binomial distribution, and hence the standard deviation of n_0 is calculated as $\sqrt{n_{all}p(1-p)}$, where p is n_0/n_{all}. Using these considerations, we calculate the average signal N and the statistical error.

The maximum value of R for the analysis, 4500 m, corresponds to ~ 15 μs for cosmic rays to pass the distance at close to the speed of light. The difference in a particle arrival time between a detector located at an air shower core position on the ground and one in the shower forwarding direction with $R = 4500$ m is ~ 21 μs for the air shower with $\theta = 55°$, which is the maximum value of θ in this
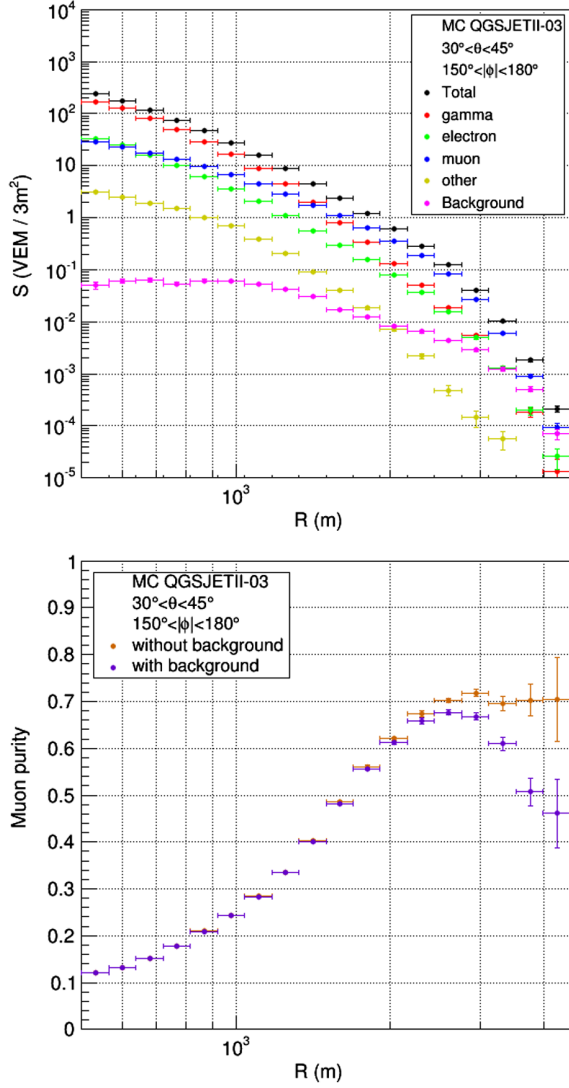
FIG. 4. (top) Lateral distributions of the air shower average signal of the MC with QGSJET II-03 for $30° < \theta < 45°$, $150° < |\phi| < 180°$, $500 \, m < R < 4500 \, m$. The red, green, blue, yellow, magenta and black represent gamma, electron, muon, other shower components, atmospheric muon background and the total of them, respectively. The vertical error bar shows the standard deviation. (bottom) Lateral distributions of the muon purity. The violet and orange show calculations with and without the atmospheric muon background, respectively.

FIG. 5. Lateral distributions of air showers of the data and the MC for $30° < \theta < 45°, 150° < |\phi| < 180°, 1500 \, m < R < 4500 \, m$. The vertical thin error bars and shaded grey thick error bars represent statistical errors and quadratic sums of statistical and systematic errors, respectively. (top) Lateral distributions of the average signal assuming the histograms follow the Poisson distribution, denoted as N in the figure. The black and red points represent the data and the MC, respectively. (bottom) The average ratio of the data to the MC.

analysis. This is shorter than the trigger time period to sample the SDs ($\pm 32 \, \mu s$); thus we assume that air shower particles reaching the SDs later than the period are negligible.

V. RESULTS

A. Comparison of data with MC

Figure 5 shows the lateral distributions of the signal and the ratio of the data to proton MC using the QGSJET II-03 hadronic interaction model. The average ratios of the data

to the MC are calculated to be $1.72 \pm 0.10 (stat) \pm 0.37 (syst)$ at $1910 \, m < R < 2160 \, m$ and $3.14 \pm 0.36 (stat) \pm 0.69 (syst)$ at $2760 \, m < R < 3120 \, m$. The systematic uncertainty is explained in Sec. V B. The observed lateral distribution falls down slower than the MC. The data become closer to the MC at $R \gtrsim 4000 \, m$, since the atmospheric muon background dominates the SD signals at the distance.

Figure 6 shows the lateral distributions of the signal and the ratio of the data to the MC with other hadronic interaction models; QGSJET II-03, QGSJET II-04, EPOS1.99 and SIBYLL2.1. The ratios of the data to the MC
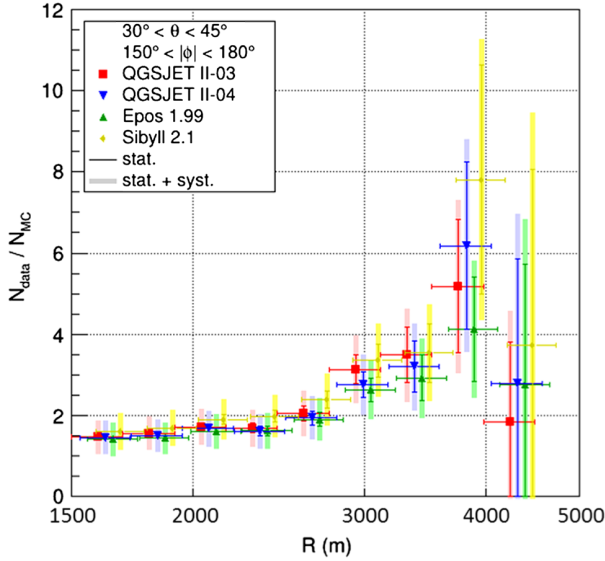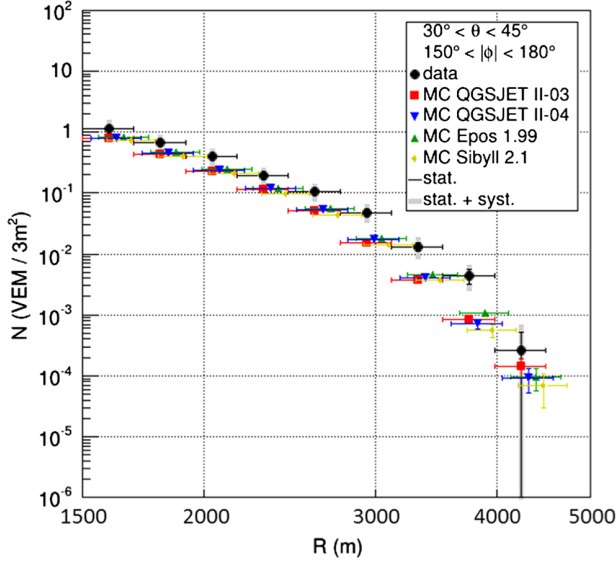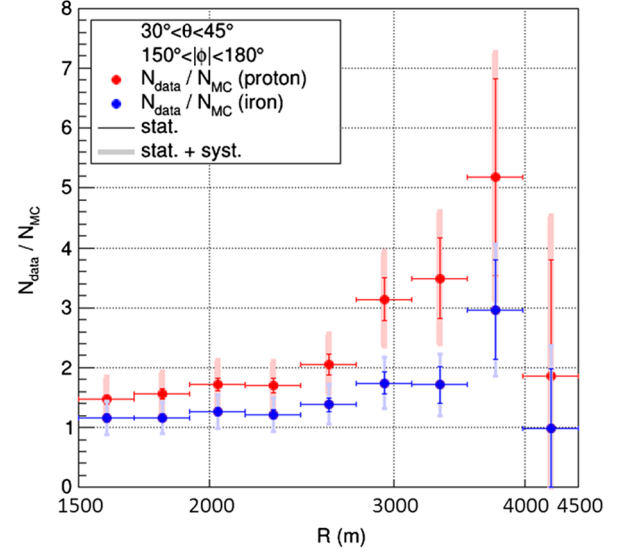
FIG. 7. Ratios of the signal size of the data to the MCs for the proton and iron. The red and blue points represent the ratios of the data to the MC for proton and that for iron, respectively. The vertical thin error bars and shaded thick error bars represent statistical errors and quadratic sums of statistical and systematic errors, respectively.

FIG. 6. Same as Fig. 5, but with the MCs using other hadronic models. (top) Lateral distributions of the average signal size assuming the histograms follow the Poisson distribution. The black, red, blue, green and yellow represent data, QGSJET II-03, QGSJET II-04, EPOS1.99 and SIBYLL2.1, respectively. To make error bars easy to see, the plots for the latter three models are shifted to the right. (bottom) The average ratio of the data to the MC. The color corresponds to MC hadronic models described in the top figure.

with QGSJET II-04 for proton are $1.67 \pm 0.10(\text{stat}) \pm 0.36(\text{syst})$ at $1910 \text{ m} < R < 2160 \text{ m}$ and $2.75 \pm 0.32(\text{stat}) \pm 0.60(\text{syst})$ at $2760 \text{ m} < R < 3120 \text{ m}$. The observed lateral distribution (circles) decreases less with radial distance than that of all hadronic interaction models (other points).

We calculated lateral distributions for iron showers using the MC with QGSJET II-03. Figure 7 shows lateral distributions of the ratio of the data to the MCs for the proton and iron. The average signal of the data is larger than the MC for iron for $R \gtrsim 2500 \text{ m}$. For the smaller distances,

the difference between the data and the MC for iron is smaller than systematic errors. Table I summarizes the results in each R.

Figure 8 shows the correlation between the muon purity expected from the MC and the ratio of the signal size of the data to that of the MC. We loosened the cut condition of the zenith angle of air showers from 45° to 55° to see the correlation precisely. On the high muon purity condition ($30° < \theta < 45°, 150° < |\phi| < 180°$, $2000 \text{ m} < R < 4000 \text{ m}$, magenta filled circle in Fig. 8), the muon purity and the ratio of the data to the MC are 65% and $1.88 \pm 0.08(\text{stat}) \pm 0.42(\text{syst})$, respectively. In the case of the low muon purity condition ($\theta < 30°, |\phi| < 30°, 2000 \text{ m} < R < 4000 \text{ m}$, black open circle in Fig. 8), they are calculated to be 28%

TABLE I. Ratio of observed SD signal sizes to MC predictions using QGSJET II-03 as a function of R. Errors due to statistical error (stat.) and systematic error (syst.) are described.

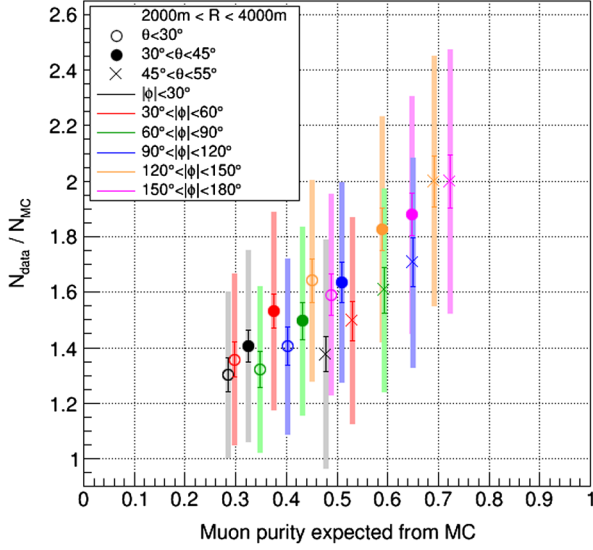| R (m)	Ratio$\pm\sigma_{\text{stat}} \pm \sigma_{\text{syst}}$	
	Proton	Iron
[1500, 1695]	$1.47^{+0.09}_{-0.08} \pm 0.35$	$1.16^{+0.07}_{-0.06} \pm 0.28$
[1695, 1915]	$1.56^{+0.09}_{-0.08} \pm 0.35$	$1.16 \pm 0.06 \pm 0.26$
[1915, 2160]	$1.72 \pm 0.10 \pm 0.37$	$1.26 \pm 0.07 \pm 0.27$
[2160, 2445]	$1.69 \pm 0.12 \pm 0.37$	$1.22 \pm 0.08 \pm 0.27$
[2445, 2760]	$2.05 \pm 0.18 \pm 0.46$	$1.38 \pm 0.11 \pm 0.31$
[2760, 3120]	$3.14 \pm 0.36 \pm 0.69$	$1.74 \pm 0.19 \pm 0.38$
[3120, 3525]	$3.49 \pm 0.68 \pm 0.86$	$1.71 \pm 0.30 \pm 0.42$
[3525, 4180]	$5.18 \pm 1.64 \pm 1.27$	$2.96 \pm 0.83 \pm 0.72$
[4180, 4500]	$1.85 \pm 1.95 \pm 1.81$	$0.99 \pm 0.99 \pm 0.96$

FIG. 8. The correlation between the muon purity and the ratio of the signal size of the data to the MC with QGSJET II-03 for 2000 m < R < 4000 m. The black, red, green, blue, orange and magenta represent $|\phi| < 30°$, $30° < |\phi| < 60°$, $60° < |\phi| < 90°$, $90° < |\phi| < 120°$, $120° < |\phi| < 150°$ and $150° < |\phi| < 180°$, respectively. The open circle, filled circle and cross represent $\theta < 30°$, $30° < \theta < 45°$ and $45° < \theta < 55°$, respectively. The vertical thin error bars and shaded thick error bars represent statistical errors and quadratic sums of statistical and systematic errors, respectively.

and $1.30 \pm 0.06(\text{stat}) \pm 0.29(\text{syst})$, respectively. This figure shows larger differences in signal sizes between the data and the MC for conditions of higher muon purity.

B. Systematic uncertainty

FD energy determination: One of the systematic uncertainties of this work is caused by the uncertainty of the TA FD energy measurement, which is 21% [21]. According to the generalized Heitler model of hadronic air showers, the number of particles from the EM and muonic components of the showers is proportional to $E^{1.03}$ and $E^{0.85}$, respectively, where E is the primary cosmic ray energy [34]. In this analysis, SD signals include both EM and muon components, with a muon fraction of 60%–70%. We conservatively assume the signal size is proportional to E and apply the systematic uncertainty of $\pm 21\%$ to the measurement.

1 MIP calibration: 1 MIP signal size is determined by fitting a histogram of single atmospheric muons and searching for the peak position of the histogram. The accuracy of this calibration method is calculated as $\epsilon_{1\text{mip}}/S_{1\text{mip}}$, where $S_{1\text{mip}}$ is the peak value of the histogram determined by fitting and $\epsilon_{1\text{mip}}$ is the fitting error of $S_{1\text{mip}}$. We calculate the average value of $\epsilon_{1\text{mip}}/S_{1\text{mip}}$ using all the SD signals in the data set to estimate the systematic error. The calculated error value is $\pm 1.2\%$.

Atmospheric muon cut: In the TA SD event reconstruction, we perform a cut on the SD signals not included in space-time clusters. This procedure reduces random atmospheric muon background in the data set. We calculated the systematic error of this procedure as the difference in the cut signal ratio between the data and the MC, that is $\pm|(S_{\text{cut}}/S_{\text{no cut}})_{\text{data}} - (S_{\text{cut}}/S_{\text{no cut}})_{\text{MC}}|/2$. Here, S_{cut} and $S_{\text{no cut}}$ are the signal before and after the cut, respectively. To avoid air shower signals affecting the calculation, we used the bin at 4000 m $\lesssim R < 4500$ m. The background in that bin is expected to be larger than each air shower component from the MC. The calculated error is $\pm 1\%$.

Poisson distribution assumption: In this analysis, we calculated the average signal from air showers with an assumption of the signal size distribution following the Poisson distribution. It is possible that these distributions do not match due to a smearing effect of signals in the SD. We calculate the systematic error from this assumption by comparing the average signal using the Poisson distribution, N, with the simple averaged value, S; $\pm|(S_{\text{data}}/S_{\text{MC}} - N_{\text{data}}/N_{\text{MC}})/(N_{\text{data}}/N_{\text{MC}})|/2$. The calculated values have R dependence and are within $\pm 4\%$.

Event reconstruction: The TA SD reconstruction procedure uses the SDs in the lateral distribution fitting without separating them by the azimuth angle. The signal size of air showers in the shower arrival direction is larger than that in the shower forwarding direction compared in the same R, and thus the reconstructed core position has a systematic shift on the side of the air shower arrival direction. If the shift of the data is different from that of the MC, it will result in a systematic error. However, we cannot compare the shift between the data and the MC since the "true" air shower geometry of the data is not given. Instead, we calculated the bias of the signal size from the shift, that is $\pm(N_{\text{in}} - N_{\text{rec}})/N_{\text{rec}}/2$, using the MC. Here, N_{rec} and N_{in} are the signal size with reconstructed event parameters (E, θ, ϕ and core position) and the same with input ones, respectively. The calculated values have R dependence and are in the range of 4%–13%. We used them as the systematic error.

SDs not working properly: The average duty cycle of the SD array is approximately 95%, and hence 5% of SDs in

TABLE II. Summary of systematic errors in the TA SD signal on the condition $30° < \theta < 45°$, $150° < |\phi| < 180°$ and 2000 m < R < 4000 m.

Source	Systematic error
FD energy determination	$\pm 21\%$
1 MIP calibration	$\pm 1.2\%$
Atmospheric muon cut	$\pm 1\%$
Poisson distribution assumption	$\pm(<4\%)$
Event reconstruction	$\pm(4\text{–}13\%)$
SDs not working properly	$\pm(<1\%)$
Total	$\pm(22\text{–}24\%)$

the event data set may be assumed to be not working properly. We calculated the average signal size with this effect removed and compared it with the measured value. The systematic uncertainty is calculated by subtracting this bias between the data and the MC. The calculated values have R dependence and are within $\pm 1\%$.

Table II summarizes all systematic errors in this work. As a result of above considerations, the energy determination uncertainty dominates the total systematic errors.

VI. DISCUSSION

In this paper, we have established a method to study muons from air showers with the TA scintillator SD. The results imply that part of the discrepancy in signal sizes between the data and the MC is due to a muon excess in the data. The measurement presented here is qualitatively consistent with the result of the Pierre Auger experiment [6,9], in which the threshold energy of muon detection ($\sim$10 MeV for TA and 300 MeV for Pierre Auger) and R conditions are different. We also found that a lateral distribution in the data falls slower than that of the MC on a high muon purity condition. It suggests the lateral distribution of muons differs between data and MCs.

Another lesson from this analysis is that the muon excess is part of the cause of an energy scale discrepancy between the TA SD and FD. Comparing the energy measured by the SD and that by the FD in the same events, we see a difference of 27% [30]. The TA FD measures an air shower energy from calorimetric fluorescence light signals, which are mostly from the EM component and less affected by the excess of muons. We use $S800$ to determine the energy with the TA SD, where $S800$ is the charge density measured at 800 m from the shower axis. Though the muon purity in SD signals is about 20% at that distance, the muon excess may partly cause misunderstanding of the conversion relation between $S800$ and the primary energy in the MC, resulting in the systematic shift of the measured energy scale.

We have used proton primaries for the MC since the results of the TA FD measurement are consistent with a light component. The Pierre Auger Collaboration indicated a mixed composition of proton and intermediate mass components in their results of FD measurements, where iron nuclei did not have a significant contribution [35]. There is a report that the TA data are compatible with the mixed composition within the systematic uncertainties [36]. Since the number of muons is larger at a heavier composition, the result in this work using the mixed composition is expected to show a similar excess between the proton and iron in Fig. 7.

VII. CONCLUSION

We have studied muons in UHECR-induced air showers detected by the TA SD. The air shower events and the locations of SDs were binned in θ, ϕ and R in order to determine events with a high muon purity. We compared air shower signals of the data with that of the MC on the high muon purity condition ($30° < \theta < 45°$, $150° < |\phi| < 180°$, 2000 m $< R <$ 4000 m) for $10^{18.8}$ eV $< E < 10^{19.2}$ eV. On that condition, the muon purity expected from the MC is $\sim$65%, and the ratios of the signal size of the data to that of the MC with QGSJET II-03 are 1.72 ± 0.10(stat) ± 0.37(syst) at 1910 m $< R <$ 2160 m and 3.14 ± 0.36(stat)$\pm$ 0.69(syst) at 2760 m $< R <$ 3120 m. The ratios for the MC with QGSJET II-04 are 1.67 ± 0.10(stat) ± 0.36(syst) and 2.75 ± 0.32(stat) ± 0.60(syst) at the same R bins. The lateral distribution of the data falls down slower than the MC on the high muon purity condition, resulting in a larger ratio of the data to the MC at larger R values. Also, the difference in the signal size between the data and the MC is larger with higher muon purity, which implies that part of the discrepancy between the data and the MC is due to an excess of muons in the data.

The primary effect found in this work, that the muon signal is larger in the data than the MC, is qualitatively consistent with the excesses of muons observed in the Pierre Auger Observatory. In addition, we found that the shape of the lateral distribution of the MC did not reproduce that found in the data. This result provides information critical to the understanding of hadronic interactions at ultrahigh energies and to improving the reliability of hadronic interaction models used in the air shower MC.

[1] M. Fukushima, Prog. Theor. Phys. Suppl. **151,** 206 (2003).

[2] T. Stroman *et al.*, Proc. Sci. ICRC2015 (**2015**) 361.

[3] T. Fujii *et al.*, Proc. Sci. ICRC2015 (**2015**) 320.

[4] T. Abu-Zayyad *et al.*, Phys. Rev. Lett. **84,** 4276 (2000).

[5] A. V. Glushkov, I. T. Makarov, M. I. Pravdin, I. E. Sleptsov, D. S. Gorbunov, G. I. Rubtsov, and S. V. Troitsky, JETP Lett. **87,** 190 (2008).

[6] A. Aab *et al.* (Pierre Auger Collaboration), Phys. Rev. D **91,** 032003 (2015); **91,** 059901(E) (2015).

[7] S. Ostapchenko, Phys. Rev. D **83,** 014018 (2011).

[8] K. Werner, F. M. Liu, and T. Pierog, Phys. Rev. C **74,** 044902 (2006).

[9] A. Aab *et al.* (Pierre Auger Collaboration), Phys. Rev. Lett. **117,** 192001 (2016).

[10] W. D. Apel *et al.*, Astropart. Phys. **95,** 25 (2017).

[11] L. G. Dedenko, A. V. Lukyashin, G. F. Fedorova, T. M. Roganova, D. Berge, A. de Roeck, M. Mangano, and B. Pattison, Eur. Phys. J. Web Conf. **99,** 10003 (2015).

[12] J. G. Gonzalez *et al.*, J. Phys. Conf. Ser. **718,** 052017 (2016).

[13] Yu. A. Fomin, N. N. Kalmykov, I. S. Karpikov, G. V. Kulikov, M. Yu. Kuznetsov, G. I. Rubtsov, V. P. Sulakov, and S. V. Troitsky, Astropart. Phys. **92,** 1 (2017).

[14] T. Abu-zayyad *et al.*, Nucl. Instrum. Methods Phys. Res., Sect. A **689,** 87 (2012).

[15] R. U. Abbasi *et al.*, Astropart. Phys. **80,** 131 (2016).

[16] D. Ivanov, Ph.D. thesis, Rutgers–The State University of New Jersey, Department of Physics and Astronomy, Piscataway, NJ, 2012.

[17] M. Takeda *et al.*, Phys. Rev. Lett. **81,** 1163 (1998).

[18] M. Takeda *et al.*, Astropart. Phys. **19,** 447 (2003).

[19] D. Heck *et al.*, Forschungszentrum Karlsruhe Report No. FZKA-6019, 1998.

[20] D. Ikeda *et al.*, Proc. Sci. ICRC2015 (**2015**) 362.

[21] T. Abu-Zayyad *et al.*, Astropart. Phys. **61,** 93 (2015).

[22] R. U. Abbasi *et al.*, Astropart. Phys. **86,** 21 (2017).

[23] A. Ferrari *et al.*, Technical Report No. 2005-010, CERN, 2005.

[24] G. Battistoni, F. Cerutti, A. Fassò, A. Ferrari, S. Muraro, J. Ranft, S. Roesler, and P. R. Sala, AIP Conf. Proc. **896,** 31 (2007).

[25] W. R. Nerson *et al.*, Technical Report No. 0265, SLAC, 1985.

[26] M. Kobal *et al.*, Astropart. Phys. **15,** 259 (2001).

[27] B. T. Stokes, R. Cady, D. Ivanov, J. N. Matthews, and G. B. Thomson, Astropart. Phys. **35,** 759 (2012).

[28] J. Allison *et al.*, IEEE Trans. Nucl. Sci. **53,** 270 (2006).

[29] R. U. Abbasi *et al.* (High Resolution Fly's Eye Collaboration), Phys. Rev. Lett. **100,** 101101 (2008).

[30] T. Abu-Zayyad *et al.*, Astrophys. J. **768,** L1 (2013).

[31] R. U. Abbasi *et al.*, Astropart. Phys. **64,** 49 (2015).

[32] T. Pierog and K. Werner, Nucl. Phys. B, Proc. Suppl. **196,** 102 (2009).

[33] E. J. Ahn, R. Engel, T. K. Gaisser, P. Lipari, and T. Stanev, Phys. Rev. D **80,** 094003 (2009).

[34] J. Matthews, Astropart. Phys. **22,** 387 (2005).

[35] A. Aab *et al.* (Pierre Auger Collaboration), Phys. Rev. D **90,** 122006 (2014).

[36] V. de Souza *et al.*, Proc. Sci. ICRC2017 (**2017**) 522.